Received 12 June 2020
Revised 3 September 2020
27 November 2020
21 December 2020
Accepted 23 December 2020

Improvement of a topological level-set approach to find optimal topology by considering body forces

Meisam Takalloozadeh
Department of Civil and Environmental Engineering, School of Engineering, Shiraz University, Shiraz, Iran, and
Gil Ho Yoon
School of Mechanical Engineering, Hanyang University, Seoul, Republic of Korea

Abstract

Purpose – Body forces are always applied to structures in the form of the weight of materials. In some cases, they can be neglected in comparison with other applied forces. Nevertheless, there is a wide range of structures in civil and mechanical engineering in which weight or other types of body forces are the main portions of the applied loads. The optimal topology of these structures is investigated in this study.

Design/methodology/approach – Topology optimization plays an increasingly important role in structural design. In this study, the topological derivative under body forces is used in a level-set-based topology optimization method. Instability during the optimization process is addressed, and a heuristic solution is proposed to overcome the challenge. Moreover, body forces in combination with thermal loading are investigated in this study.

Findings – Body forces are design-dependent loads that usually add complexity to the optimization process. Some problems have already been addressed in density-based topology optimization methods. In the present study, the body forces in a topological level-set approach are investigated. This paper finds that the used topological derivative is a flat field that causes some instabilities in the optimization process. The main novelty of this study is a technique used to overcome this challenge by using a weighted combination.

Originality/value – There is a lack of studies on level-set approaches that account for design-dependent body forces and the proposed method helps to understand the challenges posed in such methods. A powerful level-set-based approach is used for this purpose. Several examples are provided to illustrate the efficiency of this method. Moreover, the results show the effect of body forces and thermal loading on the optimal layout of the structures.

Keywords Topology optimization, Body forces, Pareto method, Topological derivative, Thermal loading

Paper type Research paper

1. Introduction

There are wide ranges of structures in which body forces comprise the main portion of the applied load. For instance, Plate 1 shows a bridge in which self-weight is significantly greater than other types of applied loads such as vehicle loading. Centrifugal force and electromagnetic and inertial forces are other common types of body forces. However,

Engineering Computations
Vol. 38 No. 8, 2021
pp. 3174-3192

0264-4401
DOI 10.1108/EC-06-2020-0324

This work was supported by Korea Institute of Energy Technology Evaluation and Planning (KETEP) grant funded by the Korea Government (MOTIE) (20202020800030, Development of Smart Hybrid Envelope Systems for Zero Energy Buildings through Holistic Performance Test and Evaluation Methods and Fields Verifications).

Plate 1.
A steel bridge in Seoul

structural optimization under body forces is a design-dependent problem. These types of problems are usually more difficult to solve than structural optimization under fixed loads. Although body forces are considered in a few studies, for most studies on topology optimization, these forces are neglected. This study uses a level-set approach to find the optimal topology of structures under body forces. The difficulties and solutions are investigated.

In topology optimization, one attempts to find the best material distribution of the continuum structures for the given objective functions and constraints in a predefined design domain. Today, this branch lies at the frontier of studies in the field of structural optimization. The application of topology optimization has expanded rapidly. Additive manufacturing has greatly contributed to this expansion. Moreover, various branches of physics and engineering are used for topology optimization. Since 1988 (Bendsoe and Kikuchi, 1988), several methods have been developed for topology optimization. There are numerous appropriate studies that review topology optimization methods (Sigmund and Maute, 2013; Eschenauer and Olhoff, 2001; Zhu *et al.*, 2020) such as the homogenization method (Hassani and Hinton, 1998a, Hassani and Hinton, 1998b), solid isotropic material and penalization (SIMP) (Bendsoe and Sigmund, 2013; Rozvany, 2001), evolutionary structural optimization (ESO), bidirectional ESO (BESO) (Huang and Xie, 2010) and level-set methods (van Dijk *et al.*, 2013). Another novel approach in topology optimization is the moving morphable component method (MMC) (Zhang *et al.*, 2016; Guo *et al.*, 2016), which uses the position and the shape of the components to define the structural layout. Moreover, this method is improved to use topological derivative (Takalloozadeh and Yoon, 2017b), therefore, the used topological derivative in this study can implement in the MMC method. Here, we restrict our attention to studies that consider body forces in topology optimization.

The first comprehensive study in which topology optimization problems, including self-weight, were investigated was conducted in 2005 by Bruyneel and Duysinx (2005).

They used the SIMP density-based method, and several difficulties were addressed in the study. The first issue is the non-monotonic behavior of compliance as the objective function. The density dependence of the loads in the SIMP method causes this non-uniformity with respect to some design variables. The second issue in including density-dependent loads is the inactive volume constraint. This problem has also been pointed out in Turteltaub and Washabaugh (1999). The third difficulty concerns using the SIMP method, which leads to parasitic effects in low-density regions. The guided weighted method used in the SIMP method and the rational approximation of material properties (RAMP) model were used to overcome these difficulties in 2013 (Xu *et al.*, 2013). They obtained clearer topologies using the RAMP model. To overcome the parasitic effects, another study developed a closed B-splines-based method (Zhang *et al.*, 2017). In this method, design variables are defined by control parameters in B-spline and are unattached to the finite element model. The minimum compliance structural topology for the loading resulting from the worst possible acceleration of the structure was obtained by Holmberg *et al.* (2015). Their study shows how the min-max problem can be formulated as a nonlinear semidefinite programming problem. In one of the latest studies in which body forces were considered (Zhang *et al.*, 2020), the authors improved the SIMP method by using the auxiliary sweep method, which is applied to the penalty factor to avoid the parasitic effect. The proposed method maintains the activeness of the prescribed volume constraint and avoids gray elements in the design domain. To consider additive manufacturing constraints such as overhang, self-weight should be involved. The porous structural pattern is produced in the contact region by easy removal of support-structures (Zhou *et al.*, 2020). In combination with the additive manufacturing filtering technique, the authors proposed a multi-field structural parameterization.

In the ESO-based method, Ansola *et al.* (2006) showed that traditional sensitivity, which had been used, does not work properly when self-weight is added. They proposed a new relation to calculate smoothing iterations during the optimization process that can overcome numerical instabilities in the traditional ESO. In another study on evolutionary methods, soft and hard kill in the BESO method was developed to account for self-weight (Huang and Xie, 2011). To find the optimum topology of trusses under the self-weight load, mixed-integer second-order cone programming was used by Kanno and Yamada (2017). The proposed approach can be readily applied to problems with discrete design variables.

A recent study investigated the optimum topology for steady and unsteady incompressible Navier-Stokes flows, including body forces (Deng *et al.*, 2018). The power-law approach was used to penalize physical body forces in the Navier-Stokes equations. Moreover, the problem was solved by level-set-based topology optimization, and the topological sensitivity was calculated using shape sensitivity based on the asymptotic analysis. Some numerical examples, such as the mass distribution of the flow local velocity with body forces, were solved. Similarly, a power-law function was used to update the element density in the topology optimization of the internal structure of an aircraft wing under a self-weight load (Félix *et al.*, 2019). An optimization framework was developed by three design fields to simultaneously find the optimal material, shape and topology (Fernandez *et al.*, 2020). By solving a dam problem, the authors showed the method can consider design-dependent loads such as self-weight.

As can be seen, few studies have addressed body forces in level-set-based topology optimization. In this study, a level-set-based method called "Pareto" is used to consider self-weight. The used method does not have the limitations of the density-based-methods. However, there is a numerical instability, and a weighted combination is used to overcome it. The Pareto method is based on a topological derivative. Topological derivatives are

powerful tools in topology optimization that allow topological changes, such as creating new holes in the domain during the optimization process (van Dijk *et al.*, 2013). This concept was proposed by Eschenauer *et al.* (1994) and has been extended later and used in topology optimization (Novotny *et al.*, 2005; Turevsky *et al.*, 2009; Suresh, 2010; Suresh, 2013). For example, a fictitious domain method was proposed in Norato *et al.* (2007) by using the topological derivative to find the optimal layout. The proposed method is efficient even when relatively coarse finite element grids mesh is used.

The following section, Section 2, defines the problem, the Pareto method and the topological derivative. Section 3 describes the implementation of a topological derivative including body forces and addresses the challenges. In Section 4, some examples are provided to validate the proposed method. The conclusion is presented in Section 5.

2. Problem definition

In Pareto topology optimization (PTO), one finds the optimum topology of multi-objective topology optimization. It can be formulated as follows (Suresh, 2010).

$$\begin{aligned} &\text{Min}_{\Omega\subset D} \quad \{J, |\Omega|\} \\ &\text{subject to} \\ &|\Omega| = |\Omega|^* \\ &\int_\Omega \boldsymbol{\sigma}(\mathbf{u}) : \boldsymbol{\varepsilon}(\boldsymbol{\eta})\, d\Omega = \int_{\Gamma_N} \mathbf{q}\cdot\boldsymbol{\eta}\, d\Gamma + \int_\Omega \mathbf{b}\cdot\mathbf{u}\, d\Omega \end{aligned} \tag{1}$$

where the strain tensor, Cauchy stress tensor and displacement field vector are denoted by $\boldsymbol{\varepsilon}(\mathbf{u})$,$\boldsymbol{\sigma}(\mathbf{u})$ and $\mathbf{u}$, respectively. The virtual displacement field $\boldsymbol{\eta}$ requires to satisfy the essential boundary conditions, that is, the Dirichlet boundary on Γ_D. Here, $\mathbf{b}$ stands for body forces. The total region of computation, the topology that must be computed and its volume are denoted by D, Ω and $|\Omega|^*$, respectively. The external force $\mathbf{q}$ is defined at the Neumann boundary (Γ_N) and the prescribed displacement $\overline{\mathbf{u}}$ is defined at the Dirichlet boundary (Γ_D) ($\mathbf{u} = \overline{\mathbf{u}}$ on Γ_D,$\boldsymbol{\sigma}(\mathbf{u})\cdot\mathbf{n} = \mathbf{q}$ on Γ_N). Moreover, half of the compliance J is defined as

$$J(\mathbf{u}) = \frac{1}{2}\int_\Omega \boldsymbol{\sigma}(\mathbf{u}) : \boldsymbol{\varepsilon}(\mathbf{u})\, d\Omega - \int_{\Gamma_N} \mathbf{q}\cdot\mathbf{u} d\Gamma - \int_\Omega \mathbf{b}\cdot\mathbf{u} d\Omega \tag{2}$$

The Pareto method traces the Pareto frontier by using the topological derivative (T) as a level-set function. The algorithm starts from the solid domain and moves on the Pareto frontier to reach the desired volume ($|\Omega|^*$) (Figure 1). In each step of the optimization process, the optimum domain is defined by Suresh (2010).

$$\Omega = \{\mathbf{x} | T(\mathbf{x}) > l\}, \quad |\Omega| = V, \tag{3}$$

where l is a scalar value that defines a cutting plane. The parts of the computation region (D) that have topological sensitivity greater than l and total volume V are defined as the optimum domain (Ω) in that step. This means that the domain Ω is the set of all regions where the topological field exceeds l. The value for the cutting plane (l) can be chosen such that a certain percentage of the volume is eliminated. In other words, the portions of the domain that are least critical for the stiffness of the structure (when the objective function is compliance) have been removed. By using this method, a pseudo-optimal domain has been constructed directly from the topological sensitivity field (Suresh and Takalloozadeh, 2013).

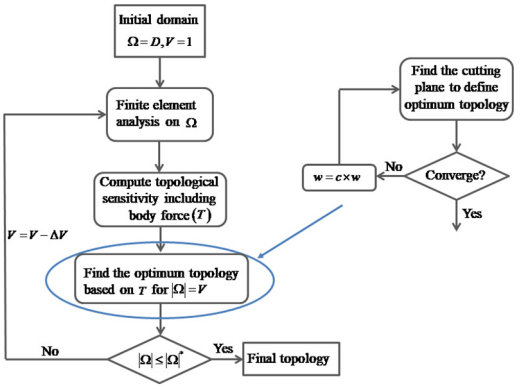

Figure 1.
PTO algorithm including body forces

To find l, a fixed-point iteration is used, and it usually converges in three to five iterations. To learn more about the proofs and the Pareto level-set-based method, see the original paper (Suresh, 2010).

2.1 Topological derivative considering body forces

Because the Pareto method uses a topological derivative as a level-set function to find the optimal domain, a brief introduction to the topological derivative is given in this section. Assume that Ω is a smooth domain of $\mathbb{R}^2$, in which Γ is its boundary. By inserting a small circular hole (B_δ) at the center, $\hat{x}$, with a radius δ, Ω is changed into a new domain, $\Omega_\delta = \Omega - \overline{B}_\delta$, as shown in Figure 2. Mathematically, the inserted circular hole and the boundary of the inserted hole are denoted by $\overline{B}_\delta = B_\delta \cup \partial B_\delta$ and ∂B_δ, respectively (Novotny *et al.*, 2003; Novotny *et al.*, 2007).

The δ index for each parameter represents that the parameter in the new domain contains a hole with radius δ. Then, the topological sensitivity can be defined as the first-order effect of this inserted hole on an objective function.

The topological derivative DT_ψ for the objective function ψ can be defined as follows:

$$D_T\psi = \lim_{\delta \to 0} \frac{\psi(\Omega_\delta) - \psi(\Omega)}{f(\delta)} \tag{4}$$

A smoothed area of a hole, $f(\delta)$, is assumed and it monotonically approaches zero when δ decreases. Equation (4) can be rewritten as (Novotny *et al.*, 2007).

$$D_T\psi = \frac{1}{f'(\delta)} \lim_{\delta \to 0} \frac{d}{d\tau} \psi(\Omega_\tau)\Big|_{\tau=0}, \tag{5}$$

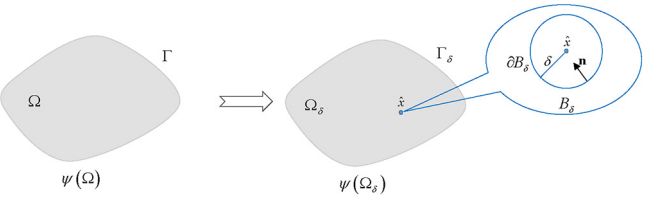

Figure 2.
Topological change resulting from insertion of a circular hole

where

$$\Omega_\tau = \{\mathbf{x}_\tau \in \mathbb{R}^2 : \mathbf{x}_\tau = \mathbf{x} + \tau\mathbf{v}, \mathbf{x} \in \Omega_\delta\}, \begin{cases} \mathbf{v} = -\mathbf{n} & \text{on } \partial B_\delta \\ \mathbf{v} = 0 & \text{on } \partial\Omega_\delta \end{cases} \tag{6}$$

Note that Ω_τ becomes Ω_δ with $\tau = 0$. The Index τ represents that the parameter is in the domain Ω_τ. The unit vector $\mathbf{n}$ is shown in Figure 2.

For a change in the total strain energy (equation (2)) with only an external load in a two-dimensional structure, the topological sensitivity can be derived as follows (Turevsky and Suresh, 2007).

$$T = \frac{4}{1+\nu}\boldsymbol{\sigma}(\mathbf{u}) : \boldsymbol{\varepsilon}(\mathbf{u}) - \frac{1-3\nu}{1-\nu^2}\mathrm{tr}\boldsymbol{\sigma}(\mathbf{u})\mathrm{tr}\boldsymbol{\varepsilon}(\mathbf{u}) \tag{7}$$

where $\boldsymbol{v}$ is Poisson's ratio. The strain tensor is defined as follows (Feng and Shi, 2013).

$$\boldsymbol{\varepsilon}(\mathbf{u}) = \frac{1}{2}(\nabla\mathbf{u} + \nabla\mathbf{u}^{\mathrm{T}}) \tag{8}$$

The topological derivative in the elastic structures under body forces can be derived similarly. The calculation is given in the Appendix. The final result is similar to that in equation (7) but with an extra term that accounts for body forces (Novotny and Sokołowski, 2013):

$$\Rightarrow T = \frac{4}{1+\nu}\boldsymbol{\sigma}(\mathbf{u}) : \boldsymbol{\varepsilon}(\mathbf{u}) - \frac{1-3\nu}{1-\nu^2}\mathrm{tr}\boldsymbol{\sigma}(\mathbf{u})\mathrm{tr}\boldsymbol{\varepsilon}(\mathbf{u}) + 2\mathbf{b}\cdot\mathbf{u} \tag{9}$$

It should be noted that the absolute values of the derivative in the design domain are not important and only the relative values are required to use in the Pareto method. Obviously, in the absence of body forces, equations 7 and 9 are similar. When gravity is applied to the structure in the opposite direction of $\hat{\mathbf{y}}$ (the unit vector), the body force is defined as

$$\mathbf{b} = -\rho g\hat{\mathbf{y}} \tag{10}$$

where ρ is the density and g is the ground gravitational acceleration.

3. Implementation in Pareto topology optimization and instability

Assume a rectangular domain with joint and hinge supports on its edges (Figure 3). The topological derivative field under the self-weight obtained by equation (9) is shown in Figure 4.

This is an almost smooth field in most parts of the domain. Because of this, the PTO algorithm cannot find the appropriate cutting plane to define the optimum layout in some steps. Recall equation (3), where the optimal domain is defined as a set of all points and regions in which the topological field exceeds the value l. Hence, it is a challenge to find the appropriate value for l such that a certain percentage of volume is placed above it. The same problem has been pointed out in applying PTO in stress-constrained topology optimization (Suresh and Takalloozadeh, 2013). To overcome this challenge and to avoid oscillation and divergence, we propose in this paper to add topological sensitivity to another desirable field when the algorithm cannot converge:

$$T_{applied} = w \times T_{calculated} + (1 - w) \times \frac{\|T_{calculated}\|}{\|\varphi\|} \times \varphi \tag{11}$$

where $\|\cdot\|$ stands for the Euclidean norm, and the value of w is equal to 1 at the beginning of the optimization and dynamically changes between 0 and 1 during the optimization process. It is updated by the coefficient $c < 1$ when the algorithm cannot converge to the desired volume fraction so $w_{new} = cw$ (Figure 1). Moreover, after finding the optimal layout for the desired volume fraction, the value w is reset to one for the next step. Here, because the topological derivative has a field similar to the stress field in general, we use the von Mises stress field as an artificial field (Lopes and Novotny, 2016):

$$\varphi = \sigma_{vonMises} \tag{12}$$

Assume a beam-like structure with material properties E =1 N/m^2, v = 0.33 and a unit vector load (F = 1N) at the top middle (Figure 5). The optimum layout obtained by PTO using the topological derivative is shown in Figure 6(a). Moreover, the optimum layout obtained via the von Mises stress field is depicted in Figure 6(b). The layouts are generally the same, although the one obtained by using the topological derivative leads to less final compliance.

Therefore, by using the von Mises field in the weighted combination with the topological derivative field, a priority is produced during steps in which the algorithm does not converge. When the topological sensitivity cannot distinguish between regions of similar

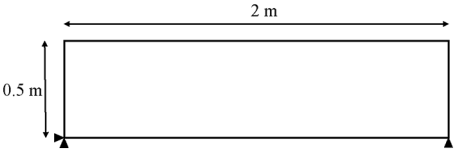

Figure 3.
Rectangular domain under self-weight

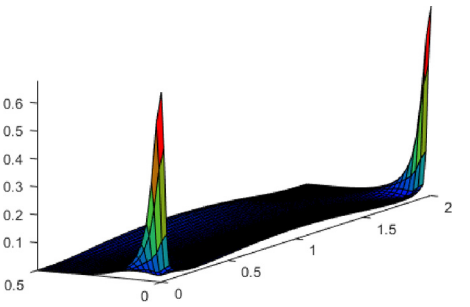

Figure 4.
Topological sensitivity in the domain under self-weight

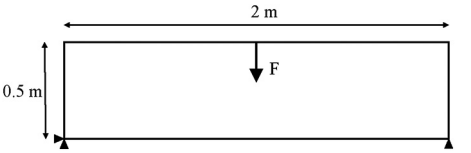

Figure 5.
Geometry and boundary conditions for the beam example

(a)

(b)

Figure 6. Optimum layout under concentrated force obtained by using the (a) topological derivative ($J = 45.4454$ N ·m) and (b) von Mises field ($J = 46.767$ N ·m)

sensitivity (smooth regions), the von Mises stress field induces a preference by eliminating the region with low von Mises stress.

Figure 7 depicts the compliance history when the PTO tries to solve the problem shown in Figure 3. The goal is to find the optimal layout with 40% volume of the initial volume. However, when the volume fraction is about 81%, the algorithm cannot converge to find the optimal layout, hence, it stops. Note that by reducing the volume, the compliance is decreased. This is because a reduction in volume leads to a decrease in the applied body force, and therefore, in the stored strain energy in the structure. The optimal layout using the proposed method is given in Figure 8 ($c\rho = 1, c_F = 0$) and discussed in Section 4.

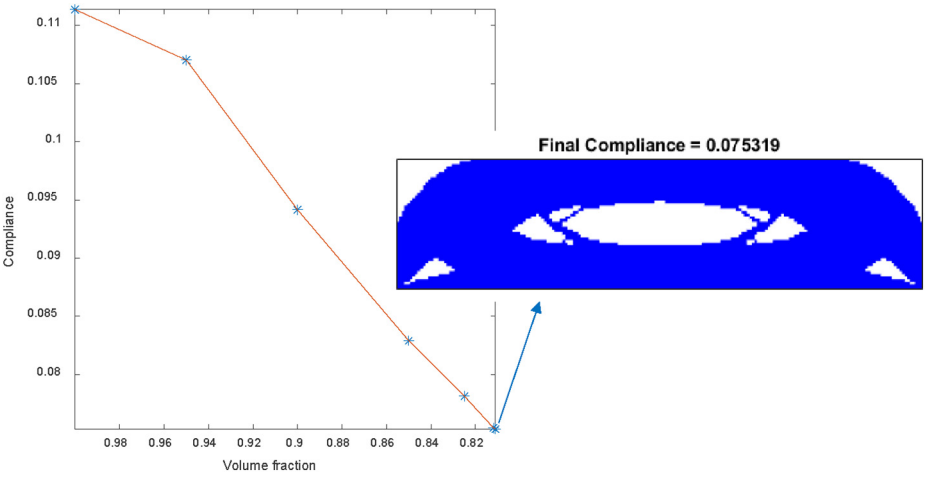

Figure 7. Compliance history and the final layout

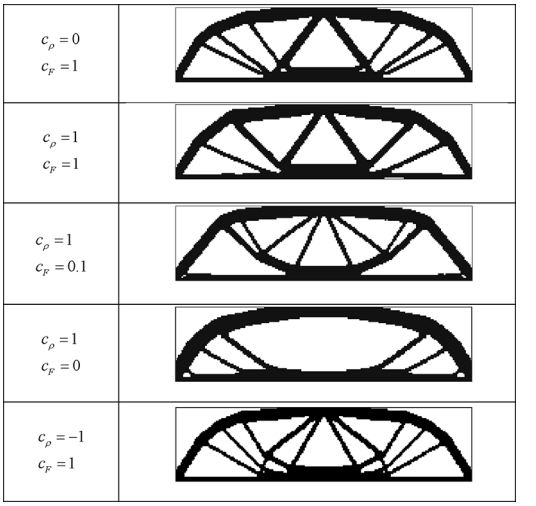

Figure 8.
Optimum topology under different loading ratios

4. Results and discussion

Several examples are provided to demonstrate the efficiency of the proposed method. The material properties of the structures in the following examples are taken as, $E = 1$, $v = 0.33$ and $\rho = 1 \times 10^{-2}$. Moreover, the coefficient c used to decrease the weight w in equation (11), is equal to 0.9.

4.1 Messerschmitt–Bolkow-Blohm beam

The optimal designs of a plane and beam-like structure under different ratios between density and concentrated force are obtained. A vertical point load is applied at the middle point of the upper side, and the domain is discretized by 10,000 elements. The final desired volume in all optimum designs is 40% of the initial one. Moreover, the maximum applied load on the center top is $F = 1$. The optimum topologies for the different cases are shown in Figure 8. To determine the effect of the body force on the optimum topology, the applied force and density are defined as follows:

$$\begin{aligned} \rho_{applied} &= c_\rho \rho \\ F_{applied} &= c_F F \end{aligned} \tag{13}$$

The optimum layout is not dependent on either the absolute values of the concentrated force ($F_{applied}$) or the density ($\rho_{applied}$) but on the ratio between them. By decreasing the concentrated load, the two bars in the middle of the beam disappeared. As can be seen, the optimum layout under self-weight is similar to an arch shape (Figure 8: $c_\rho = 1$, $c_F = 0$). The compliance values for the optimal layouts are given in Table 1-third column.

Table 1.
Compliance values in the optimum layouts

c_ρ	C_F	Compliance (N · m)	Compliance for the first optimum layout (N · m)
0	1	45.4454	45.4454
1	1	47.6457	47.7705
1	0.1	0.71306	0.7199
1	0	0.024574	0.0366

Assume the optimum layout obtained under the concentrated force (Figure 8: $c_\rho = 0$, $c_F = 1$) is still the optimal layout when we add body forces. If it is true, the compliance when the layout is reanalyzed under body forces should be less than our obtained values. The compliance values are computed and listed in the fourth column of Table 1. As expected, the optimum layouts obtained by the modified PTO have lower compliance values.

The last row in Figure 8 depicts the optimal layout when in addition to concentrated load, self-weight is applied in the opposite direction. The final compliance is obtained 42.31 N · m, which is less than 47.65 N · m, compliance for the optimal layout when gravity and concentrated load are in the same direction (Figure 8: $c_\rho = 1$, $c_F = 1$). When the applied loads are in the same direction, total deformation and total stored strain energy are more.

4.2 Square beam

The second example is that of a square plane with supports at its corners (Figure 9). The optimal design with 40% of the initial volume and just under self-weight is shown in Figure 10. The optimum layout is two arch shapes with some connection bars between them. It is interesting that the arch shape is a common optimum shape that appears in different structural optimization problems.

4.3 Body forces and thermal effects

Thermal effects are considered in topology optimization as heat transfer (Bruns, 2007; Iga *et al.*, 2009; Zhou *et al.*, 2016) or thermal stress in addition to mechanical stress (Gao and Zhang, 2010). Both are design dependent problems. For the next application, we add topological sensitivity under body forces to the thermal topological sensitivity. The calculations can be found in Giusti *et al.* (2013) and the final relation for uniform thermal change is as follows (Takalloozadeh and Yoon, 2017a):

$$T = \frac{4}{1+\nu}\boldsymbol{\sigma}(\mathbf{u}) : \boldsymbol{\varepsilon}(\mathbf{u}) - \frac{1-3\nu}{1-\nu^2}\mathrm{tr}\boldsymbol{\sigma}(\mathbf{u})\mathrm{tr}\boldsymbol{\varepsilon}(\mathbf{u}) - \frac{2\alpha\theta}{1-\nu}\mathrm{tr}\boldsymbol{\sigma}(\mathbf{u}) - \frac{2E\alpha^2\theta^2}{1-\nu} + 2\mathbf{b}\cdot\mathbf{u} \tag{14}$$

where α is the thermal expansion coefficient and θ is the thermal change. Assume a clamped beam (Figure 11) with the same material properties as in the previous examples

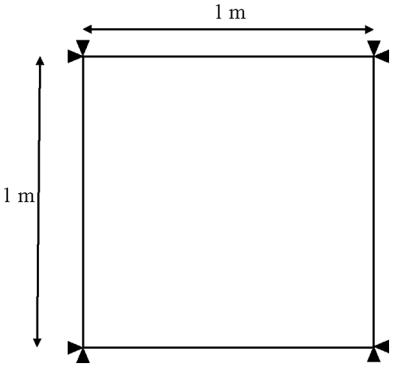

Figure 9.
Design domain

Figure 10.
Optimum layout

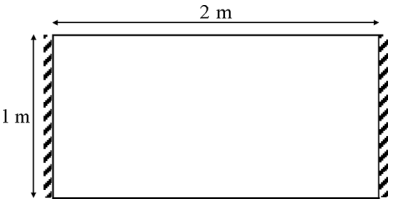

Figure 11.
Clamped beam problem

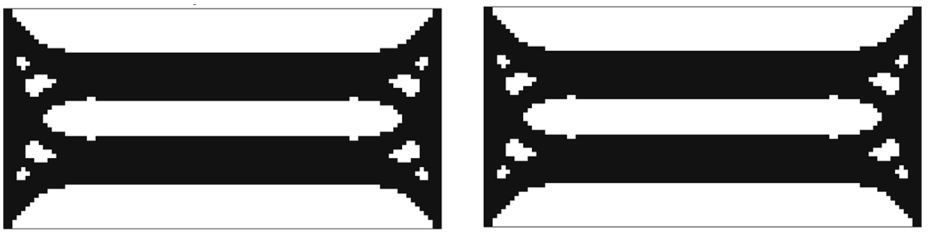

Figure 12.
Optimum topology of the clamped beam under only thermal load: (a) $\theta = 10°$; (b) $\theta = -10°$

and $\alpha = 1 \times 10^{-2}$. The optimum layouts for this domain with uniform increasing and decreasing temperatures of 10° and −10° are shown in Figures 12(a) and 12(b), respectively. The obtained topology and compliance value for both elevated and decreased temperatures are the same ($J = 0.017734\ \mathrm{N \cdot m}$).

A unit concentrated force is applied at the center of the beam, and the optimum layouts under temperature changes are obtained again (Figure 13). Both layouts have the same compliance ($J = 4.6355\ \mathrm{N} \cdot \mathrm{m}$), but with an inverse shape. The optimum topologies under the same temperature changes and self-weight are shown in Figure 14. As can be seen in Figures 13 and 14, the optimum layouts have an arch with downward and upward curvature for the elevated and decreased temperatures, respectively. This shape leads to less compliance when a downward load (self-weight or concentrated force) is applied to the beam.

4.4 Three-dimensional topology optimization

The topological derivative for three-dimensional linear problems can be obtained by using (Novotny *et al.*, 2007):

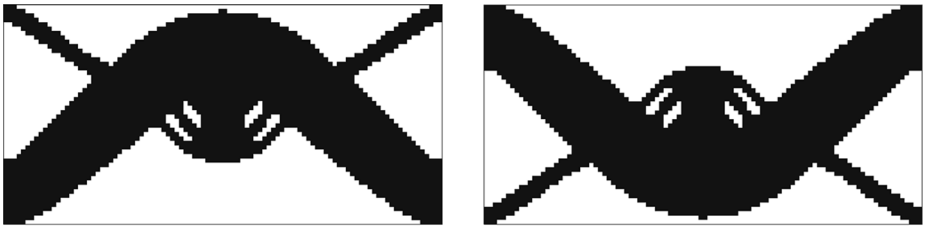

(a) **(b)**

Figure 13.
Optimum topology of the clamped beam under concentrated force $F = 1$ and thermal load: (a) $\theta = 10°$; (b) $\theta = -10°$

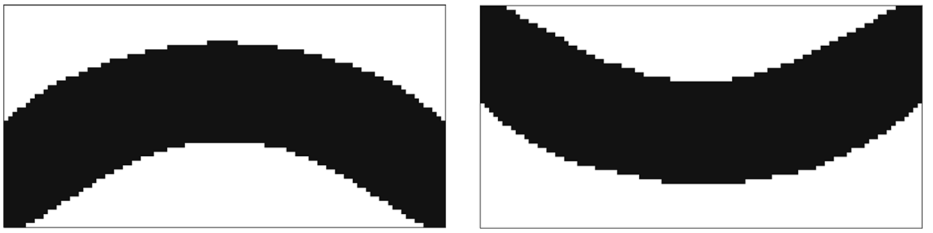

(a) **(b)**

Figure 14.
Optimum topology of the clamped beam under the body force and thermal load: (a) $\theta = 10°$; (b) $\theta = -10°$

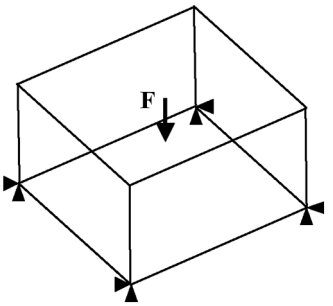

Figure 15.
Initial domain

$$T = \frac{3}{4}\frac{1-\nu}{7-5\nu}\left[10\boldsymbol{\sigma}(\mathbf{u}) : \boldsymbol{\varepsilon}(\mathbf{u}) - \frac{1-5\nu}{1-2\nu}\mathrm{tr}\boldsymbol{\sigma}(\mathbf{u})\mathrm{tr}\boldsymbol{\varepsilon}(\mathbf{u})\right] \tag{15}$$

This formula is modified underbody forces by an extra term:

$$T_{BodyForce} = T - \mathbf{b} \cdot \mathbf{u} \tag{16}$$

An initial cubic model ($2\,\mathrm{m}^3 \times 2\,\mathrm{m}^3 \times 1\,\mathrm{m}^3$) with material properties $E = 1\mathrm{N/m}^2$ and $v = 0.33$ and a unit vector load ($F = 1\mathrm{N}$) at the top middle is assumed (Figure 15). The final volume is set to 20% of the initial volume. Figure 16 shows the optimum layouts under a concentrated force with coarse and finer meshes. The results under the body force and using equation (16) are shown in Figure 17. Once again, the obtained layout under self-weight consists of several arches.

5. Conclusion

Body forces are considered in topology optimization by using a powerful level-set-based method called Pareto. For this purpose, a topological derivative is used to solve the multi-objective compliance-volume minimization problem. However, the topological derivative field considering body forces usually flattens out far away from regions of

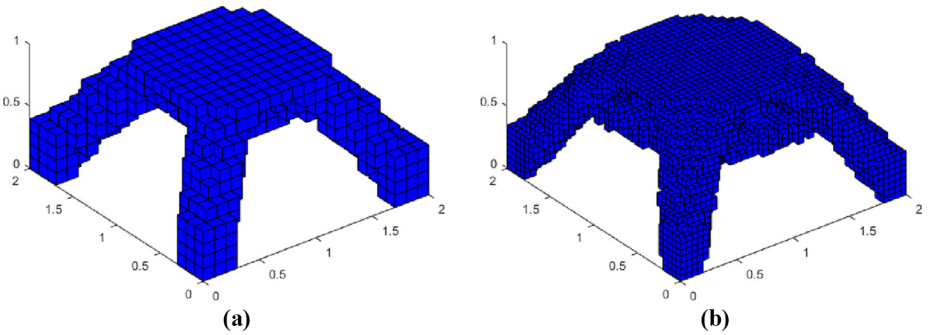

Figure 16.
Optimum layouts under concentrated force (for different element sizes)

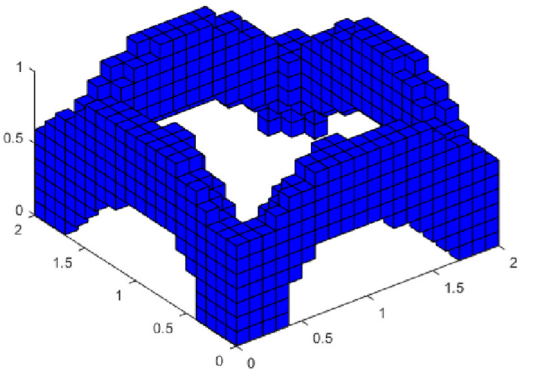

Figure 17.
Optimum layout under self-weight

high sensitivity. This poses a numerical instability during level-set extraction. To overcome this challenge in a few steps, a new field is used by combining the topological sensitivity field and the von Mises stress field. By means of a weighted combination, a priority is produced during steps in which the algorithm does not converge. When the topological derivative cannot distinguish between regions of similar sensitivity (flat regions), the von Mises stress field induces a preference by eliminating the region with low von Mises stress. Several two- and three-dimensional examples were solved, and the results proved the ability of the proposed method. It should be noted that the final layout may depend somewhat on the selected weight in the proposed heuristic combination. The obtained layouts demonstrate the efficiency of the weighted combination to overcome the instability issue. Moreover, the simultaneous effects of body forces and thermal loads can be considered by using the proposed method. As a repetitive design, an arch shape typically appeared in the optimum layouts of the structures under self-weight loads. Future work will focus on including hydrostatic pressure as a design-dependent load by using a topological derivative.

References

Ansola, R., Canales, J. and Tárrago, J.A. (2006), "An efficient sensitivity computation strategy for the evolutionary structural optimization (ESO) of continuum structures subjected to self-weight loads", *Finite Elements in Analysis and Design*, Vol. 42 Nos 14/15, pp. 1220-1230.

Bendsoe, M.P. and Kikuchi, N. (1988), "Generating optimal topologies in structural design using a homogenization method".

Bendsoe, M.P. and Sigmund, O. (2013), *Topology Optimization: theory, Methods, and Applications*, Springer Science and Business Media.

Bruns, T.E. (2007), "Topology optimization of convection-dominated, steady-state heat transfer problems", *International Journal of Heat and Mass Transfer*, Vol. 50 Nos 15/16, pp. 2859-2873.

Bruyneel, M. and Duysinx, P. (2005), "Note on topology optimization of continuum structures including self-weight", *Structural and Multidisciplinary Optimization*, Vol. 29 No. 4, pp. 245-256.

Deng, Y., Wu, Y. and Liu, Z. (2018), "Topology optimization for fluid flows with body forces", *Topology Optimization Theory for Laminar Flow*, Springer.

Eschenauer, H.A. and Olhoff, N. (2001), "Topology optimization of continuum structures: a review", *Applied Mechanics Reviews*, Vol. 54 No. 4, pp. 331-390.

Eschenauer, H.A., Kobelev, V.V. and Schumacher, A. (1994), "Bubble method for topology and shape optimization of structures", *Structural Optimization*, Vol. 8 No. 1, pp. 42-51.

Félix, L. Gomes, A.A. and Suleman, A.J.E.O. (2019), "Topology optimization of the internal structure of an aircraft wing subjected to self-weight load", pp. 1-17.

Feng, K. and Shi, Z.C. (2013), *Mathematical Theory of Elastic Structures*, Springer Science and Business Media.

Fernandez, F., Barker, A.T., Kudo, J., Lewicki, J.P., Swartz, K., Tortorelli, D.A., Watts, S., White, D.A. and Wong, J. (2020), "Simultaneous material, shape and topology optimization", *Computer Methods in Applied Mechanics and Engineering*, Vol. 371, p. 113321.

Gao, T. and Zhang, W. (2010), "Topology optimization involving thermo-elastic stress loads", *Structural and Multidisciplinary Optimization*, Vol. 42 No. 5, pp. 725-738.

Giusti, S.M., Novotny, A., Rivera, J.M. and Rodriguez, J.E. (2013), "Strain energy change to the insertion of inclusions associated to a thermo-mechanical semi-coupled system", *International Journal of Solids and Structures*, Vol. 50 No. 9, pp. 1303-1313.

Guo, X., Zhang, W., Zhang, J. and Yuan, J. (2016), "Explicit structural topology optimization based on moving morphable components (MMC) with curved skeletons", *Computer Methods in Applied Mechanics and Engineering*, Vol. 310, pp. 711-748.

Hassani, B. and Hinton, E. (1998a), "A review of homogenization and topology optimization I – homogenization theory for media with periodic structure", *Computers and Structures*, Vol. 69, pp. 707-717.

Hassani, B. and Hinton, E. (1998b), "A review of homogenization and topology optimization II – analytical and numerical solution of homogenization equations", *Computers and Structures*, Vol. 69, pp. 719-738.

Holmberg, E., Thore, C.J. and Klarbring, A. (2015), "Worst-case topology optimization of self-weight loaded structures using semi-definite programming", *Structural and Multidisciplinary Optimization*, Vol. 52 No. 5, pp. 915-928.

Huang, X. and Xie, Y.M. (2010), "A further review of ESO type methods for topology optimization", *Structural and Multidisciplinary Optimization*, Vol. 41 No. 5, pp. 671-683.

Huang, X. and Xie, Y. (2011), "Evolutionary topology optimization of continuum structures including design-dependent self-weight loads", *Finite Elements in Analysis and Design*, Vol. 47 No. 8, pp. 942-948.

Iga, A., Nishiwaki, S., Izui, K. and Yoshimura, M. (2009), "Topology optimization for thermal conductors considering design-dependent effects, including heat conduction and convection", *International Journal of Heat and Mass Transfer*, Vol. 52 Nos 11/12, pp. 2721-2732.

Kanno, Y. and Yamada, H. (2017), "A note on truss topology optimization under self-weight load: mixed-integer second-order cone programming approach", *Structural and Multidisciplinary Optimization*, Vol. 56 No. 1, pp. 221-226.

Lopes, C.G. and Novotny, A.A. (2016), "Topology design of compliant mechanisms with stress constraints based on the topological derivative concept", *Structural and Multidisciplinary Optimization*, Vol. 54 No. 4, pp. 737-746.

Norato, J.A., Bendsøe, M.P., Haber, R.B. and Tortorelli, D.A. (2007), "A topological derivative method for topology optimization", *Structural and Multidisciplinary Optimization*, Vol. 33 Nos 4/5, pp. 375-386.

Novotny, A.A., FeijÓOo, R.A., Padra, C. and Taroco, E. (2005), "Topological derivative for linear elastic plate bending problems", *Control and Cybernetics*, Vol. 34, pp. 339-361.

Novotny, A.A., Feijóo, R.A., Taroco, E. and Padra, C. (2003), "Topological sensitivity analysis", *Computer Methods in Applied Mechanics and Engineering*, Vol. 192 Nos 7/8, pp. 803-829.

Novotny, A., Feijóo, R., Taroco, E. and Padra, C. (2007), "Topological sensitivity analysis for three-dimensional linear elasticity problem", *Computer Methods in Applied Mechanics and Engineering*, Vol. 196 Nos 41/44, pp. 4354-4364.

Novotny, A.A. and Sokołowski, J. (2013), *Topological Derivatives in Shape Optimization*, Springer-Verlag Berlin Heidelberg.

Parkus, H. (2012), *Thermoelasticity*, Springer Science and Business Media.

Rozvany, G.I.N. (2001), "Aims, scope, methods, history and unified terminology of computer-aided topology optimization in structural mechanics", *Structural and Multidisciplinary Optimization*, Vol. 21 No. 2, pp. 90-108.

Sigmund, O. and Maute, K. (2013), "Topology optimization approaches a comparative review", *Structural and Multidisciplinary Optimization*, Vol. 48 No. 6, pp. 1031-1055.

Suresh, K. (2010), "A 199-line matlab code for pareto-optimal tracing in topology optimization", *Structural and Multidisciplinary Optimization*, Vol. 42 No. 5, pp. 665-679.

Suresh, K. (2013), "Efficient generation of large-scale pareto-optimal topologies", *Structural and Multidisciplinary Optimization*, Vol. 47 No. 1, pp. 49-61.

Suresh, K. and Takalloozadeh, M. (2013), "Stress-constrained topology optimization: a topological level-set approach", *Structural and Multidisciplinary Optimization*, Vol. 48 No. 2, pp. 295-309.

Takalloozadeh, M. and Yoon, G.H. (2017a), "Development of pareto topology optimization considering thermal loads", *Computer Methods in Applied Mechanics and Engineering*, Vol. 317, pp. 554-579.

Takalloozadeh, M. and Yoon, G.H. (2017b), "Implementation of topological derivative in the moving morphable components approach", *Finite Elements in Analysis and Design*, Vol. 134, pp. 16-26.

Turevsky, I. and Suresh, K. (2007), "Generalization of topological sensitivity and its application to defeaturing", *ASME IDETC conference*, *Las Vegas*.

Turevsky, I., Gopalakrishnan, S.H. and Suresh, K. (2009), "An efficient numerical method for computing the topological sensitivity of arbitrary-shaped features in plate bending", *International Journal for Numerical Methods in Engineering*, Vol. 79 No. 13, pp. 1683-1702.

Turteltaub, S. and Washabaugh, P. (1999), "Optimal distribution of material properties for an elastic continuum with structure-dependent body force", *International Journal of Solids and Structures*, Vol. 36 No. 30, pp. 4587-4608.

VAN Dijk, N.P., Maute, K., Langelaar, M. and VAN Keulen, F. (2013), "Level-set methods for structural topology optimization: a review", *Structural and Multidisciplinary Optimization*, Vol. 48 No. 3, pp. 437-472.

Xu, H.Y., Guan, L.W., Chen, X. and Wang, L.P. (2013), "Guide-weight method for topology optimization of continuum structures including body forces", *Finite Elements in Analysis and Design*, Vol. 75, pp. 38-49.

Zhang, S., Li, H. and Huang, Y. (2020), "An improved multi-objective topology optimization model based on SIMP method for continuum structures including self-weight", *Structural and Multidisciplinary Optimization*, pp. 1-20.

Zhang, W., Zhao, L. and Gao, T. (2017), "CBS-based topology optimization including design-dependent body loads", *Computer Methods in Applied Mechanics and Engineering*, Vol. 322, pp. 1-22.

Zhang, W., Yuan, J., Zhang, J. and Guo, X. (2016), "A new topology optimization approach based on moving morphable components (MMC) and the ersatz material model", *Structural and Multidisciplinary Optimization*, Vol. 53 No. 6, pp. 1243-1260.

Zhou, M., Liu, Y. and Wei, C. (2020), "Topology optimization of easy-removal support structures for additive manufacturing", *Structural and Multidisciplinary Optimization*, Vol. 61 No. 6.

Zhou, M., Alexandersen, J., Sigmund, O. and Pedersen, C.B. (2016), "Industrial application of topology optimization for combined conductive and convective heat transfer problems", *Structural and Multidisciplinary Optimization*, Vol. 54 No. 4, pp. 1045-1060.

Zhu, B., Zhang, X., Zhang, H., Liang, J., Zang, H., Li, H. and Wang, R. (2020), "Design of compliant mechanisms using continuum topology optimization: a review", *Mechanism and Machine Theory*, Vol. 143, p. 103622.

Appendix

The weak form of the mechanical equilibrium equation is as follows:

$$\int_{\Omega} \boldsymbol{\sigma}(\mathbf{u}) : \boldsymbol{\varepsilon}(\boldsymbol{\eta})\, d\Omega = \int_{\Gamma_N} \mathbf{q} \cdot \boldsymbol{\eta}\, d\Gamma + \int_{\Omega} \mathbf{b} \cdot \mathbf{u}\, d\Omega (\mathbf{u} = \overline{\mathbf{u}} \quad \text{on } \Gamma_D, \boldsymbol{\sigma}(\mathbf{u}) \cdot \mathbf{n} = \mathbf{q} \quad \text{on } \Gamma_N) \tag{17}$$

The above equation is valid on the domain with a hole, Ω_δ, as well as on the domain with an expanded hole, Ω_τ and the associated boundaries. The Cauchy stress is expressed as follows:

$$\boldsymbol{\sigma}(\mathbf{u}) = \mathbf{C}\boldsymbol{\varepsilon}(\mathbf{u}) \tag{18}$$

where the elastic coefficient tensor is $\mathbf{C} = \mathbf{C}^{\mathrm{T}}$. With body forces, the equilibrium equation can be rewritten as:

$$div\,\boldsymbol{\sigma}(\mathbf{u}) + \mathbf{b} = 0 \quad \text{in } \Omega, \Omega_\delta, \text{ and } \Omega_\tau \tag{19}$$

The weak form of equation (19) in the domain Ω_δ with a hole with radius δ is written as follows:

$$\int_{\Omega_\delta} \boldsymbol{\sigma}(\mathbf{u}_\delta) : \boldsymbol{\varepsilon}(\boldsymbol{\eta}_\delta) d\Omega = \int_{\Gamma_N} \mathbf{q} \cdot \boldsymbol{\eta}_\delta d\Gamma + \int_{\Omega_\delta} \mathbf{b} \cdot \mathbf{u}_\delta d\Omega \tag{20}$$

The total potential energy ($\psi(\Omega_\tau) = J(\mathbf{u}_\tau)$), can be determined as follows:

$$J(\mathbf{u}_\tau) = \frac{1}{2}\int_{\Omega_\tau} \mathbf{C}\boldsymbol{\varepsilon}(\mathbf{u}_\tau) : \boldsymbol{\varepsilon}(\mathbf{u}_\tau)\, d\Omega - \int_{\Gamma_N} \mathbf{q} \cdot \mathbf{u}_\tau d\Gamma - \int_{\Omega_\tau} \mathbf{b} \cdot \mathbf{u}_\tau d\Omega$$

(using equation (18))(21)

From the Reynolds transport theorem, the derivative $J(\mathbf{u}_\tau)$ with respect to time can be summarized as follows:

$$\frac{d}{d\tau} J(\mathbf{u}_\tau)\Big|_{\tau=0} = \frac{1}{2}\int_{\partial\Omega_\delta} (\boldsymbol{\sigma}(\mathbf{u}_\delta) : \boldsymbol{\varepsilon}(\mathbf{u}_\delta))(\mathbf{v} \cdot \mathbf{n})\, d\Gamma + \frac{1}{2}\int_{\Omega_\tau} \frac{\partial}{\partial \tau} (\boldsymbol{\sigma}(\mathbf{u}_\tau) : \boldsymbol{\varepsilon}(\mathbf{u}_\tau))\Big|_{\tau=0} d\Omega$$
$$-\int_{\Gamma_N} \mathbf{q} \cdot \dot{\mathbf{u}}_\delta\, d\Gamma - \int_{\partial\Omega_\delta} (\mathbf{b} \cdot \mathbf{u}_\delta)(\mathbf{v} \cdot \mathbf{n})\, d\Gamma - \int_{\Omega_\tau} \frac{\partial}{\partial \tau} (\mathbf{b} \cdot \mathbf{u}_\tau)\Big|_{\tau=0} d\Omega \tag{22}$$

The relation between $\dot{\mathbf{u}}_\delta$ and $\mathbf{u}'_\delta$ can be expressed as follows:

$$\dot{\mathbf{u}}_\delta = \frac{d}{d\tau}\mathbf{u}_\delta = \frac{\partial}{\partial \tau}\mathbf{u}_\delta + \frac{\partial \mathbf{u}_\delta}{\partial \mathbf{x}_\tau}\frac{\partial \mathbf{x}_\tau}{\partial \tau} = \mathbf{u}'_\delta + (\nabla \mathbf{u}_\delta)\mathbf{v} = \mathbf{u}'_\delta + \mathbf{w}_\delta \tag{23}$$

Therefore, the derivative in the second term on the right side of equation (22) can be written as:

$$\frac{\partial}{\partial \tau} (\boldsymbol{\sigma}(\mathbf{u}_\tau) : \boldsymbol{\varepsilon}(\mathbf{u}_\tau))\Big|_{\tau=0} = 2\boldsymbol{\sigma}(\mathbf{u}_\delta) : \boldsymbol{\varepsilon}(\dot{\mathbf{u}}_\delta) - 2\boldsymbol{\sigma}(\mathbf{u}_\delta) : \boldsymbol{\varepsilon}(\mathbf{w}_\delta) \tag{24}$$

$\dot{\mathbf{u}}_\delta$ can be considered as an arbitrary displacement field ($\boldsymbol{\eta}_\delta$) in equation (20) by substituting the above relation into equation (22):

$$\frac{d}{d\tau} J(\mathbf{u}_\tau)\Big|_{\tau=0} = \frac{1}{2}\int_{\partial\Omega_\delta} \left(\boldsymbol{\sigma}(\mathbf{u}_\delta) : \boldsymbol{\varepsilon}(\mathbf{u}_\delta) - \mathbf{b} \cdot \mathbf{u}_\delta\right)(\mathbf{v} \cdot \mathbf{n}) d\Gamma - \int_{\Omega_\delta} \boldsymbol{\sigma}(\mathbf{u}_\delta) : \boldsymbol{\varepsilon}(\mathbf{w}_\delta)$$
$$- \int_{\Omega_\delta} \mathbf{b} \cdot \mathbf{w}_\delta d\Omega \tag{25}$$

By considering the shape change velocity field ($\mathbf{v}$) as defined in equation (6), as well as $\boldsymbol{\sigma}(\mathbf{u}_\delta)\,\boldsymbol{n} = 0$ on ∂B_δ, the summation of the second and third terms on the right side of equation (25) is zero:

$$\int_{\Omega_\delta} \boldsymbol{\sigma}(\mathbf{u}_\delta) : \boldsymbol{\varepsilon}(\mathbf{w}_\delta) d\Omega + \int_{\Omega_\delta} \mathbf{b} \cdot \mathbf{w}_\delta d\Omega = \int_{\partial\Omega_\delta} \boldsymbol{\sigma}(\mathbf{u}_\delta)\mathbf{w}_\delta \cdot \mathbf{n} - \int_{\Omega_\delta} div(\boldsymbol{\sigma}(\mathbf{u}_\delta)) \cdot \mathbf{w}_\delta$$
$$+ \int_{\Omega_\delta} \mathbf{b} \cdot \mathbf{w}_\delta d\Omega = \int_{\partial\Omega_\delta} \boldsymbol{\sigma}(\mathbf{u}_\delta)\mathbf{w}_\delta \cdot \mathbf{n} = \int_{\partial\Omega_\delta} \boldsymbol{\sigma}(\mathbf{u}_\delta)(\nabla \mathbf{u}_\delta)\mathbf{v} \cdot \mathbf{n} = \int_{\partial B_\delta} \boldsymbol{\sigma}(\mathbf{u}_\delta)(\nabla \mathbf{u}_\delta)\mathbf{v} \cdot \mathbf{n} d\Gamma$$
$$= 0 \tag{26}$$

Therefore,

$$\frac{d}{d\tau} J(\mathbf{u}_\tau)|_{\tau=0} = -\frac{1}{2}\int_{\partial B_\delta} \left(\boldsymbol{\sigma}(\mathbf{u}_\delta) : \boldsymbol{\varepsilon}(\mathbf{u}_\delta) - 2\mathbf{b} \cdot \mathbf{u}_\delta\right) d\Gamma \tag{27}$$

Finally, the required derivative in equation (5) is obtained as follows:

$$D_T \psi = \lim_{\delta \to 0} \frac{1}{f'(\delta)} \left(-\frac{1}{2}\int_{\partial B_\delta} \left(\boldsymbol{\sigma}(\mathbf{u}_\delta) : \boldsymbol{\varepsilon}(\mathbf{u}_\delta) - \mathbf{b} \cdot \mathbf{u}_\delta\right) \right) \tag{28}$$

By using the inverse of the tensor of the elastic coefficient $\left(\mathbf{C}^{-1} = \frac{1}{E}\left[(1+\nu)\mathbf{II} - \nu(\mathbf{I} \otimes \mathbf{I})\right]\right)$ to define the strain tensor in terms of the stress tensor, the following expression can be obtained:

$$D_T \psi = \lim_{\delta \to 0} \frac{1}{f'(\delta)} \left(-\frac{1}{2}\int_{\partial B_\delta} \left(\frac{1}{E}\left[(1+\nu)\boldsymbol{\sigma}(\mathbf{u}_\delta) : \boldsymbol{\sigma}(\mathbf{u}_\delta) - \nu(\mathrm{tr}\boldsymbol{\sigma}(\mathbf{u}_\delta))^2\right] \right) d\Gamma \right) \tag{29}$$

Note that the identity matrix is **I, II** is the fourth-order identity tensor and the symbol $\otimes$ indicates the tensor product. To calculate the above integration on boundary ∂B_δ, the stress tensor needs to be decomposed as:

$$\boldsymbol{\sigma}(\mathbf{u}_\delta)|_{\partial B_\delta} = \sigma_\delta^{nn}(\mathbf{n} \otimes \mathbf{n}) + \sigma_\delta^{tn}(\mathbf{t} \otimes \mathbf{n}) + \sigma_\delta^{nt}(\mathbf{n} \otimes \mathbf{t}) + \sigma_\delta^{tt}(\mathbf{t} \otimes \mathbf{t}) \tag{30}$$

where $\mathbf{n}$ and $\mathbf{t}$ are normal and tangential vectors on the boundary, respectively, and ∂B_δ and σ^{ij} are the related stresses in these directions. The boundary conditions on ∂B_δ are as follows:

$$\boldsymbol{\sigma}(\mathbf{u}_\delta)\mathbf{n} = \sigma_\delta^{nn}\mathbf{n} + \sigma_\delta^{tn}\mathbf{t} = 0 \Rightarrow \sigma_\delta^{nn} = \sigma_\delta^{tn} = 0 \quad \text{on } \partial B_\delta \tag{31}$$

Therefore,

$$D_T \psi = \lim_{\delta \to 0} \frac{1}{f'(\delta)} \left(-\frac{1}{2E}\int_{\partial B_\delta} \left((\sigma_\delta^{tt})^2 \right) d\Gamma \right) \tag{32}$$

Using elasticity equations for the asymptotic expansion of σ_δ^{tt} on ∂B_δ gives the resultant of the above integration (Parkus, 2012):

$$D_T\psi = \frac{1}{2E}\left[(\sigma_1+\sigma_2)^2 + 2(\sigma_1-\sigma_2)^2 + \mathbf{b}\cdot\mathbf{u}\right] \tag{33}$$

where σ_1 and σ_2 are the principal stresses at $\hat{x}$ and can be calculated as follows.

$$\sigma_{1,2} = \frac{1}{2}\left(\mathrm{tr}\boldsymbol{\sigma}(\mathbf{u}) \pm \sqrt{2\boldsymbol{\sigma}^D(\mathbf{u}) : \boldsymbol{\sigma}^D(\mathbf{u})}\right), \quad \boldsymbol{\sigma}^D(\mathbf{u}) = \boldsymbol{\sigma}(\mathbf{u}) - \frac{1}{2}(\mathrm{tr}\boldsymbol{\sigma}(\mathbf{u}))\mathbf{I} \tag{34}$$

Substituting the above relation into equation (33) yields:

$$\begin{aligned} D_T\psi &= \frac{1}{2E}\left[(\mathrm{tr}\boldsymbol{\sigma}(\mathbf{u}))^2 + 2\left(2\boldsymbol{\sigma}^D(\mathbf{u}) : \boldsymbol{\sigma}^D(\mathbf{u})\right)^2 + \mathbf{b}\cdot\mathbf{u}\right] \\ &= \frac{1}{2E}\left[(\mathrm{tr}\boldsymbol{\sigma}(\mathbf{u}))^2 + 4\left(\boldsymbol{\sigma}(\mathbf{u}) - \frac{1}{2}(\mathrm{tr}\boldsymbol{\sigma}(\mathbf{u}))\mathbf{I}\right) : \left(\boldsymbol{\sigma}(\mathbf{u}) - \frac{1}{2}(\mathrm{tr}\boldsymbol{\sigma}(\mathbf{u}))\mathbf{I}\right) + \mathbf{b}\cdot\mathbf{u}\right] \\ \Rightarrow D_T\psi &= \frac{1}{2E}\left[4\boldsymbol{\sigma}(\mathbf{u}) : \boldsymbol{\sigma}(\mathbf{u}) - (tr\boldsymbol{\sigma}(\mathbf{u}))^2 + \mathbf{b}\cdot\mathbf{u}\right] \end{aligned} \tag{35}$$

Finally, after some simplifications, we get:

$$\Rightarrow D_T\psi = T = \frac{4}{1+\nu}\boldsymbol{\sigma}(\mathbf{u}) : \boldsymbol{\varepsilon}(\mathbf{u}) - \frac{1-3\nu}{1-\nu^2}\mathrm{tr}\boldsymbol{\sigma}(\mathbf{u})\mathrm{tr}\boldsymbol{\varepsilon}(\mathbf{u}) + 2\mathbf{b}\cdot\mathbf{u} \tag{36}$$

Corresponding author
Meisam Takalloozadeh can be contacted at: takalloozadeh@shirazu.ac.ir